Clays and Clay Minerals, Vol. 50, No. 5, 633–646, 2002.

EXPERIMENTAL INVESTIGATION OF THE INTERACTION OF CLAYS WITH HIGH-pH SOLUTIONS: A CASE STUDY FROM THE CALLOVO-OXFORDIAN FORMATION, MEUSE-HAUTE MARNE UNDERGROUND LABORATORY (FRANCE)

FRANCIS CLARET[1,2], ANDREAS BAUER[3], THORSTEN SCHÄFER[3], LISE GRIFFAULT[2] AND BRUNO LANSON[1,*]

[1] Environmental Geochemistry Group, LGIT - Maison des Géosciences, University J. Fourier – CNRS, BP 53, 38041 Grenoble Cedex 9, France

[2] ANDRA, Parc de Croix Blanche, 1-7 rue Jean Monnet, 92298 Châtenay-Malabry Cedex, France

[3] Forschungszentum Karlsruhe, Institut für Nukleare Entsorgung, PO Box 3640, D-76021 Karlsruhe, Germany

Abstract—The impact of alkaline solutions (pH = 13.2) on the clay mineralogy of the Callovo-Oxfordian formation hosting the French underground laboratory for nuclear waste disposal investigation (Meuse-Haute Marne site) has been studied experimentally. Initially, each of the four samples selected as representative of the mineralogical transition in this Callovo-Oxfordian formation consists of a mixture of three main clay phases: discrete illite, discrete smectite and a randomly interstratified mixed-layered mineral (MLM) containing ~65% of non-expandable layers. Clay separates were altered in batch reactors at 60°C using high solution:solid ratios. The mineralogy of this clay fraction and solution chemistry were monitored as a function of reaction time. In addition, the interactions between organic matter and clay particles were investigated using scanning transmission X-ray microscopy (STXM).

The clay mineralogy is little affected even though the pH is still high after 1 y reaction time. The only significant mineralogical evolution is the partial dissolution of the discrete smectite component leading to the formation of a new randomly interstratified illite-expandable MLM. Additional mineralogical transformations lead, for one sample, to the dissolution of micro-crystalline quartz and, for another sample, to the crystallization of a tobermorite-like phase. The low reactivity of clay minerals may be attributed to the presence of organic matter in the samples. In their initial state, all outer surfaces of clay particles are indeed covered with organic matter. After 1 y reaction time, STXM studies showed the basal surfaces of clay particles to be devoid of organic matter, but their edges, which are the most reactive sites, were still protected.

Key Words—High pH, French Underground Laboratory, Organic Matter, STXM, XRD.

INTRODUCTION

Nuclear waste disposal in deep geological formations is currently under investigation in several countries. Based on a directive of December 31st 1991, France is conducting research in a clay-rich formation, the 'Callovo-Oxfordian argilite', in the Meuse-Haute Marne site (MHM, Eastern Paris basin). An underground laboratory will soon be operational allowing investigation of the confinement properties of this host formation. However, disposal in such deep environments demands technical solutions which ensure that waste is stored in a safe way preventing harmful effects to the population. In particular, concrete is often thought of as a civil engineering material in such deep storage facilities or as a component of the waste package, especially for intermediate-level long-lived waste (ILLW – 'B type' according to the French nuclear waste classification). However, the water-induced alteration of concrete generates alkali-rich high-pH (12.5–13.6) solutions (Anderson *et al*., 1989; Lunden and Andersson, 1989), the release of which to the surrounding media has been modeled (Jeffries *et al*., 1988; Haworth *et al*., 1989; Berner, 1990; Reardon, 1990; Vieillard and Rassineux, 1992). Such modeling shows that solution composition is first controlled by the release of NaOH and KOH leading to very high solution pH (pH >13). In a second step, the solution composition is controlled by portlandite ($Ca(OH)_2$ – pH 12), and finally by calcium-silicate-hydrate (CSH) phases (pH 9–10).

As a consequence, numerous investigations have been conducted on the stability of clays in such high pH conditions (Mohnot *et al*., 1987; Carroll-Webb and Walther, 1988; Carroll and Walther, 1990; Chermak, 1992, 1993; Eberl *et al*., 1993; Huang, 1993; Bauer and Berger, 1998; Bauer *et al*., 1998; Bauer and Velde, 1999; Cama *et al*., 2000; Taubald *et al*., 2000; Huertas *et al*., 2001). These studies consistently indicate that the clay minerals described in the Callovo-Oxfordian formation of the MHM site (smectite, illite and mixed-layer illite-smectite – Bouchet and Rassineux, 1997; Claret, 2001) would react when in contact with high-pH alkali-rich solutions. For example, recent high-pH experimental investigations on smectite-type minerals indicated a fast montmorillonite-to-beideillite transformation (Rassineux *et al*., 2001). On the other hand, the bulk mineralogy of the formation offers a good buffering capacity, especially in the presence of silicates such as quartz (~20 wt.%) and of carbonates. Similar studies on natural formations such as in the Maqarin analog site depict an

* E-mail address of corresponding author:
bruno.lanson@obs.ujf-grenoble.fr

alteration halo restricted to a few mm thick along a conducting fracture (Cassagnabere *et al*., 2001).

The main objective of this study was to investigate the specific behavior of the natural clay mineral assemblages from the Callovo-Oxfordian formation in the MHM site when in contact with Ca-Na-K-rich solutions at high pH (>13). The experimental work was conducted on <2 μm clay separates. These reactive size fractions were altered hydrothermally in closed systems for periods varying from 1 day to 1 y. Both fluids and solids were recovered and analyzed.

MATERIALS

Starting materials

The French underground laboratory will be located in Bure (eastern Paris Basin), between the Haute-Marne and Meuse departments. This laboratory will be hosted in the Callovo-Oxfordian formation the burial depth of which ranges from 422 to 552 m in the exploration drill hole EST 104. This clay formation is a hard shale containing 40–45% clay minerals, and ~50% of calcite and quartz. Bouchet and Rassineux (1997) showed that this clay formation included a mineralogical transition from smectitic 'R0' mixed-layered minerals (MLM) at the top of the formation to more illitic 'R1' MLM in its deeper section. In the sampled well, EST 104, four core samples were selected at 447, 490, 494 and 516 m below ground level as being representative of the whole mineralogical sequence covered by the clay formation. Two 'R0' samples were chosen, the first with a high smectite content (~65%) and the other one with ~50% smectite in the 'R0'. These I-S compositions were estimated from the method developed by Inoue *et al*. (1989). Another two samples were selected in the 'R1' part of the drillhole, the first one with ~60% illite, and the other with ~70% illite. These compositions were estimated from X-ray diffraction (XRD) patterns using the criteria defined by Velde *et al*. (1986). Their chemical composition was determined by Bouchet and Rassineux (1997), and additional analyses of S and C in the starting material were performed using a LECO-125 C/S analyzer. The total organic matter (TOC) and the S concentration in the initial solids are given in Table 1, the organic matter having been described exhaustively by Faure *et al*. (1999). Because organic matter is known to react with alkali solutions, particular attention was paid to this component.

Table 1. Total organic carbon (TOC) and sulfur content (wt.%) of the initial clay samples.

Sample	TOC	Sulfur
447	1.32	0.2439
490	1.31	0.2133
494	1.32	0.135
516	1.36	0.2596

Before extracting the <2 μm size-fraction by centrifugation, carbonates were removed using the acetic acid-acetate buffer method described by Moore and Reynolds (1989), but organic matter was not removed before size fractionation. Finally the clays were saturated with Ca. The mineralogy of the clay samples was investigated in detail by XRD (Claret, 2001) and scanning electron microscopy (SEM). All four clay samples consist of a mixture of three main phases: discrete illite, discrete smectite and a randomly interstratified mixed-layer mineral (MLM) containing ~65% of non expandable illite layers (Table 2; Claret, 2001). As a function of burial depth, the relative proportion of smectite decreases from 20 to 2% whereas that of discrete illite increases from 15 to 25%. The relative amount of the MLM phase (65%), as well as its composition, remains unchanged throughout the depth profile (Table 2; Claret, 2001). As a consequence, the mineralogical transition initially described, as for a diagenetic series, by a progressive illitization of I-S MLMs, corresponds to the progressive removal of discrete smectite with increasing depth together with the progressive increase of a discrete illite component.

Small amounts of kaolinite, chlorite and/or quartz may also exist in the different samples, sample 447 showing the highest concentration of quartz, which is detectable even in the $\leqslant 0.2$ μm size-fraction.

Starting solution

The simple young fluid (SYF) chemical composition is typical of solutions resulting from the initial stages of cement alteration (Nagra, 1995). The starting solutions were prepared from analytical reagent grade KOH, NaOH and $Ca(OH)_2$ salts. The solution composition and the initial pH are given in Table 3.

EQ3 (Wolery, 1983) calculations were performed to determine the distribution of aqueous species in solution in the absence of CO_2. At the initial pH, the solution is slightly oversaturated with respect to portlandite (log Q/K = 0.407). The starting solutions were nevertheless clear and showed no evidence of precipitation with time, when not exposed to air.

Table 2. Mineralogical composition of the clay (<2 μm) size-fraction of the initial clay samples as determined by Claret (2001) from experimental XRD profile fitting using the multi-specimen technique (Sakharov *et al*., 1999).

Sample	Smectite		MLM		Illite		Kaolinite	Chlorite
	%Sm	Ab.	%Sm	Ab.	%Sm	Ab.	Ab.	Ab.
447	100	20	65	65	5	15	0	0
490	100	13	65	66	5	20	0	1
494	100	2	65	74	5	19	4	1
516	100	2	65	63	5	23	9	2

The data were derived from the characterization of the Ca-saturated and EG-solvated samples. %Sm indicates the relative proportion of expandable layers in randomly interstratified mixed-layer minerals (MLM). Ab. indicates the relative proportion of the various phases in the clay fraction.

Experimental set-up and sample preparation

Clay samples weighing 0.5 g were added to 10 mL [liquid/solid ratio (L/S) = 20] and 40 mL (L/S = 80) of SYF solution. Batch experiments were performed for up to 12 months at 60°C in Savilex containers. The temperature control was precise to ±2°C and accurate to ±4°C. The bottles were shaken twice a week. The containers were removed at specific intervals, quenched in cold water (25°C), and opened. After the experiments, the reacted material and the solution were separated by centrifugation. The supernatant suspensions were filtered through a 0.45 μm filter before analysis.

The solids were then washed six times with bidistilled water (Milli-Q/18.2 MΩ cm^{-1}). After each washing step the solid was separated by centrifugation and resuspended in 50 mL Milli-Q water. In the next step the clays were re-suspended in 50 mL of 1 M $SrCl_2$ solution in order to ensure the presence of two water layers in the expandable interlayers. To promote complete cation exchange, the suspensions were stored for 4 h at 50°C. Following the cation exchange, the clays were dialyzed in tubes prepared by boiling in distilled water for one day with repeated changes of the water to remove any excess organic material.

METHODS

X-ray diffraction

Oriented slides were prepared by pipetting a slurry of the Sr-saturated samples on a glass side and drying it at 40°C for a few hours to obtain an air-dried (AD) preparation. Ethylene glycol (EG) solvation was achieved by exposing the oriented clay slides to ethylene glycol vapor at 70°C for 12 h. The XRD patterns were recorded with a Bruker D5000 diffractometer using a 0.04° step size and 6 s counting time per step. The divergence slit, two Soller slits, antiscatter slit and resolution slit were 0.5°, 2.3°, 2.3°, 0.5° and 0.06°, respectively.

To characterize the structural modification of the reacted clay samples, their structure was determined using the multi-specimen fitting procedure described by Sakharov *et al*. (1999). This method, which may be used to describe complex polyphasic clay parageneses, requires the recording of XRD patterns of each sample after different treatments (*e.g.* Sr-saturated in AD and EG solvated states). For each XRD pattern, structural parameters such as the composition of the MLM phases (proportions of the different layer types), their stacking mode (Reichweite parameter R, junction probabilities), and an estimate of their relative proportions are adjusted to fit the experimental XRD pattern (Sakharov *et al*., 1999; Claret, 2001). Because the different treatments may change the thickness and scattering power (nature, amount and position of interlayer species) of the swelling interlayers but not the distribution of the different 2:1 layer types, a consistent structural model is obtained for one sample when the structural parameters obtained from all XRD patterns of the same sample coincide.

Table 3. Composition of the Simple Young Fluid (SYF) and the initial solution pH.

NaOH	2.606 g/L
KOH	9.033 g/L
$Ca(OH)_2$	0.166 g/L
pH	13.22

To fit the experimental XRD patterns, the program of Drits and Sakharov (1976) was used over the 2–50°2θ CuKα range. Instrumental and experimental factors such as horizontal and vertical beam divergences, goniometer radius, dimensions and thickness of the samples were measured and introduced. The sigmastar value was set to 12 and the mass absorption coefficient (μ*) to 45, as recommended by Moore and Reynolds (1989). The *Z* coordinates of atoms proposed by Moore and Reynolds (1989) were used for all 2:1 layer types. The d_{001}-values used for simulations are given in Table 4. The K content in the illite interlayers was set at 0.75 atoms per $O_{10}(OH)_2$. The lognormal thickness distributions of coherent scattering domain sizes (CSDS) were characterized by the mean and maximum CSDS (Drits *et al*., 1997).

Scanning electron microscopy, scanning transition X-ray microscopy

Scanning electron microscope (SEM) images of untreated and reacted materials were recorded to identify minor components which may not be detected by XRD and to determine the relative stability of the different reaction products. These micrographs were obtained using a JEOL GSM-6100 instrument equipped with a KEVEX energy dispersive detector.

Scanning transmission X-ray microscopy (STXM) investigations were performed at beamline X1-A of the National Synchrotron Light Source (Brookhaven National Laboratory) operated by the State University of New York at Stony Brook. The principle of the method is described in detail in Jacobsen *et al*. (1991) and Zhang *et al*. (1994). Sample preparation was performed by squeezing 1 μL of aqueous colloid suspensions between Si_3N_4 windows, using a wet-cell assembly to maintain the hydration state (Neuhäusler *et*

Table 4. *d*-spacings (d_{001}) (in Å) of the different layer types used for the calculation of mixed-layer mineral XRD patterns.

	Illite	Smectite 2 layers	Smectite 1 layer
Ethylene glycol solvated	9.98	16.65–16.7	12.9–13.3
Air-dried state	9.98	14.8–15	12.5–12.8

al., 1999). Initial clay samples (⩽2 μm size-fraction) were kept in suspension in deionized water, whereas reacted samples were kept in suspension in reacted SYF.

The Fresnel zone plate used for these measurements had a diameter of 160 μm and a outermost zone width of 45 nm giving a theoretical lateral resolution of 55 nm (Rayleigh criterion), at a focal length of 1.7 mm (Spector *et al.*, 1997). The exit and entrance slit set-up was chosen to obtain an energy resolution ΔeV of 0.1 eV at the C K-edge (Winn *et al.*, 1996). Energy calibration of the spherical grating monochromator was performed by using the photon energy of the CO_2 gas adsorption band at 290.74 eV (Ma *et al.*, 1991; Hitchcock and Mancini, 1994).

The STXM images of clay suspensions were recorded at the C K-edge and K L-edge. The STXM measurements yield information on the product of sample thickness (d) and of its mass absorption coefficient $\mu(E)$ through the relation $Abs(E) = \mu(E)*d = \ln[I_0(E)/I(E)]$ in which $I_0(E)$ is the incident flux on the sample and $I(E)$ the flux measured behind the sample at the energy E. $I_0(E)$ is obtained from regions free of particles or from XANES spectra measured without sample. Low-resolution image stacks can be measured as a function of energy.

High-resolution images were collected at selected energies below and above C (E_{below} = 280 eV, E_{above} = Σ(285–290 eV)) and K (E_{below} = Σ(280–290 eV), E_{above} = 297.3 eV) edges. Ratio images were subsequently calculated giving to each pixel the corresponding $-\log(Abs_{E_{above}}/Abs_{E_{below}})$ ratio to visualize the distribution of K and C, to image the association between clay and organic matter in untreated and reacted samples (Figure 1).

In addition, X-ray absorption near-edge structure (XANES) spectra were extracted from low-resolution image stacks in the 280–310 eV range after a careful stack alignment (Jacobsen *et al.*, 2000). In the XANES spectra, clay minerals are identified using the X-ray absorption of structural interlayer K, and more precisely the absorption band double feature at 297.3 eV (L_3-edge) and 300 eV (L_2-edge). These energy values are shifted by 3 eV as compared to the values tabulated for K by Henke *et al.* (1993), because potassium is present as K^+ in these interlayers.

For XANES comparison, all spectra were corrected for the baseline and normalized to the absorption intensity of the K L_3-edge energy (297.3 eV).

Determination of solution composition

The pH was measured using an Orion 525A pH meter calibrated with five standard solutions (pH 7, 9, 10, 11, 13). Because pH measurement of high-pH solutions is always critical, each measured value was checked against a pH 13 standard. A maximum drift of ±0.1 pH unit was observed during pH measurements.

The concentrations of dissolved Si, Al, Na, K, Ca and Fe were determined for all samples on a Plasma 400

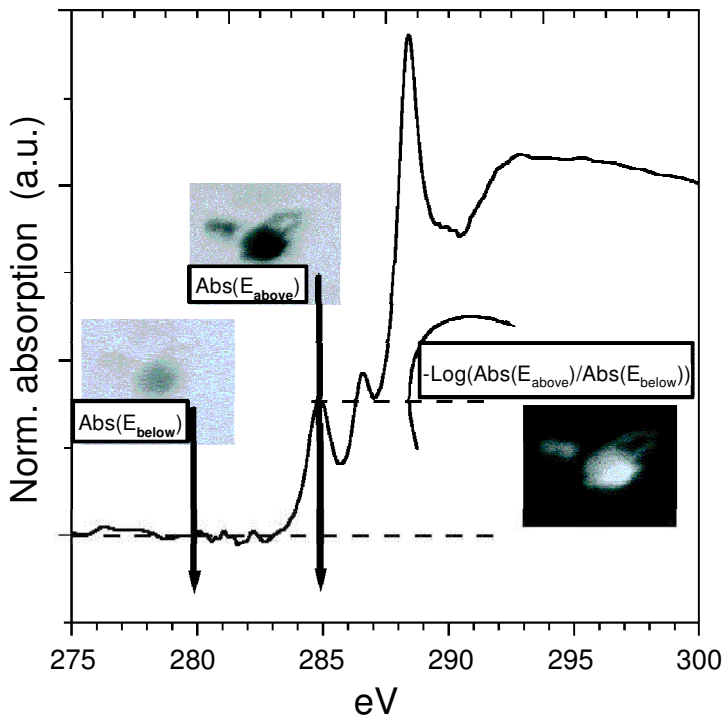

Figure 1. Absorption of a smectite suspension in organic-containing solution. The image collected at E_{below} illustrates the very limited absorption of this dilute suspension of thin smectite particles. The ratio-image $-\log(Abs_{E_{above}}/Abs_{E_{below}})$ allows us to localize specifically organic functional groups absorbing, in this case, at 285 eV.

Table 5. Concentration of the different aqueous species as a function of time.

Reaction time (days)	pH	Si (mg/L)	Al (mg/L)	Na (mg/L)	K (mg/L)	DOC (mg/L)	Sulfate (mg/L)
Sample 447 L/S 20							
1	13.17	53.7	14.4	1433.6	4632.0	30.3	29.5
3	13.15	193.6	12.5	1452.7	4416.0	46.9	52.8
6	13.21	348.5	9.4	1402.0	4113.0	67.2	79.2
9	13.16	500.0	7.6	1426.7	4186.0	80.3	92.0
16	13.13	1101.0	5.8	1411.0	4138.0	101.9	92.4
30	13.09	1512.6	5.7	1408.4	4148.0	132.8	100.3
74	12.97	2139.0	5.4	1498.0	4489.0	170.1	132.0
145	12.56	2720.8	5.3	1466.6	4645.8	229.1	145.5
350	12.25	4134.5	6.2	1472.0	4427.0	269.5	181.4
Sample 490 L/S 20							
2	13.21	53.0	14.8	1452.7	4289.0	27.3	27.3
4	13.21	79.7	24.6	1405.1	3995.0	36.6	36.8
9	13.18	99.2	32.9	1448.0	4226.0	76.8	59.4
16	13.17	139.4	41.1	1436.2	4190.0	110.5	80.4
30	13.13	158.1	46.2	1451.0	4148.0	131.8	120.4
74	13.1	215.0	54.8	1499.5	4289.0	139.6	145.0
145	13.06	334.2	48.4	1498.0	4268.4	147.8	192.0
350	13.04	269.5	49.4	1492.4	4057.6	150.9	195.1
Sample 494 L/S 20							
1	13.19	33.2	11.6	1494.5	4603.0	15.3	13.9
3	13.2	62.0	23.2	1422.3	4450.0	20.0	18.4
6	13.21	86.3	33.5	1422.0	4330.0	34.0	23.4
9	13.2	100.2	42.7	1428.8	4254.0	42.8	28.2
16	13.19	136.9	48.2	1422.6	4267.0	73.6	36.6
30	13.19	142.3	57.7	1439.6	4326.0	92.1	54.7
74	13.18	144.2	73.1	1484.1	4356.0	110.4	78.0
145	13.08	195.7	73.8	1457.6	4425.8	134.2	79.4
350	13.04	223.7	76.2	1418.0	4286.2	180.1	81.7
Sample 516 L/S 20							
1	13.22	31.2	21.0	1417.8	4913.0	21.1	22.6
3	13.19	46.6	29.6	1435.7	5156.0	23.1	41.3
6	13.22	70.4	50.2	1462.1	4157.0	60.9	68.0
9	13.25	82.2	65.7	1469.3	4378.0	48.0	99.1
16	13.22	93.4	92.5	1447.3	4404.0	76.2	118.2
30	13.22	118.6	114.1	1481.0	4480.0	99.1	149.9
74	13.2	159.4	148.8	1497.0	4789.0	101.0	201.0
150	13.09	176.9	162.0	1498.0	4662.0	113.4	219.9
350	13.05	141.4	191.8	1491.6	5083.8	119.5	239.9
Sample 447 L/S 80							
1	13.24	7.7	7.1	1507.1	5301.0	17.2	10.0
3	13.22	50.5	10.2	1482.7	5079.0	20.8	21.3
6	13.2	142.9	11.3	1504.9	5059.0	28.6	25.8
9	13.18	227.6	11.1	1492.7	4890.0	32.8	28.2
16	13.18	385.3	10.5	1504.6	4721.0	37.2	33.9
30	13.17	826.9	11.6	1509.2	4978.0	45.5	36.9
74	13.16	997.0	15.4	1467.6	4813.0	67.4	44.0
145	12.98	1225.4	7.6	1503.0	4950.6	77.9	51.6
350	12.95	1835.0	6.5	1506.4	5165.4	81.8	55.9
Sample 490 L/S 80							
1	13.21	11.4	7.3	1434.4	5243.0	10.3	7.5
3	13.21	21.0	11.4	1483.1	5048.0	10.5	11.9
6	13.18	34.4	16.3	1495.7	5496.0	10.4	13.3
9	13.21	47.4	23.7	1479.2	4861.0	12.9	18.5
16	13.19	71.9	29.0	1512.7	4766.0	26.9	21.3
30	13.17	80.9	33.7	1514.9	4849.0	34.9	24.6
74	13.16	128.3	55.2	1451.5	4859.0	47.8	34.0
145	13.17	180.4	54.1	1453.8	5342.4	57.8	44.5
350	13.14	233.1	79.2	1472.6	5058.0	66.6	47.3

Table 5. (*Contd.*)

Reaction time (days)	pH	Si (mg/L)	Al (mg/L)	Na (mg/L)	K (mg/L)	DOC (mg/L)	Sulfate (mg/L)
Sample 494 L/S 80							
1	13.23	7.2	6.3	1463.1	5000.0	6.9	3.5
3	13.21	19.1	12.5	1466.6	4945.0	7.7	5.1
6	13.23	32.0	18.3	1420.7	4978.0	11.3	8.7
9	13.22	46.1	25.1	1509.1	4918.0	14.7	11.2
16	13.21	53.8	29.0	1492.3	4771.0	20.5	13.3
30	13.23	59.7	35.2	1511.8	4906.0	24.5	14.8
74	13.24	90.8	60.9	1495.0	4886.0	28.4	18.0
145	13.16	124.0	55.8	1457.2	5042.4	37.3	17.3
350	13.15	131.4	76.4	1443.4	5424.8	48.8	20.8
Sample 516 L/S 80							
1	13.21	9.5	12.5	1482.7	5206.0	5.3	11.6
3	13.22	12.7	14.1	1468.0	5156.0	8.3	13.8
6	13.21	26.6	22.7	1444.0	5009.0	14.6	18.5
9	13.23	33.1	29.9	1519.6	5139.0	20.4	20.9
16	13.2	52.9	42.8	1506.9	4935.0	25.7	24.0
30	13.24	62.4	66.4	1514.7	4956.0	32.0	33.5
74	13.22	100.1	116.5	1411.3	4933.0	36.1	46.0
145	13.16	160.6	135.4	1461.0	5248.8	46.4	50.7
350	13.16	141.1	164.8	1477.0	5257.2	47.9	55.9

ICP-AES (Perkin Elmer) after appropriate dilution. The sulfate concentrations were determined using a DX-300 ion chromatograph. The dissolved organic carbon (DOC) was measured using a Shimadzu TOC-5000, after appropriate dilution, and pH adjustment with concentrated HCl (pH 2–3).

To determine the size distribution of released colloidal material, the reacted solutions were passed through polyethersulfone membranes of nominal molecular weight cut off ranging from 10^3 to 10^6 Dalton (Microsep™ Microconcentrators). Each filter was washed 15 times with Milli-Q water before use.

EXPERIMENTAL RESULTS

Solutions

All reacted solutions showed a change in color during the experiment. This change was not the same for the different samples, and was most intense for sample 447. For this sample, the solution was dark brownish after 74 days and opaque at the end of the experiment (L/S = 20). Filtration through a 0.45 μm filter for solution analysis purposes did not modify this strong coloration. Even after ultra-filtration through a 10^3 Dalton filter (1 nm) the solution still showed a dark brownish color, which is induced by colloidal organic material.

Dissolved organic carbon and sulfate. A similar evolution of DOC and sulfate concentrations was observed for all samples (Table 5). With increasing reaction time, the positive slope of these concentration curves decreased, maximum DOC concentration (270 mg/L) being obtained for sample 447 (L/S = 20) at the end of the experiment (350 days). The DOC was the dominant species in solution for the two L/S ratios except for sample 516 for which the solution is dominated by sulfate for the two L/S ratios. Maximum sulfate concentration (240 mg/L) was found in sample 516 (L/S 20) after 350 days (Table 5).

To determine the size distribution of this colloidal organic material as a function of reaction time, reacted solutions were filtered through polyethersulfone membranes, and DOC was measured in the filtrate and compared with the initial DOC in solution. The evolution of this size distribution as a function of time was the same for all four samples, the average size of the organic material decreasing with increasing reaction time, independently of L/S ratio (Figure 2). For example, in sample 516 (L/S = 80) ~50% and 80% of the initial DOC was present in the filtrate of a 1000 Dalton

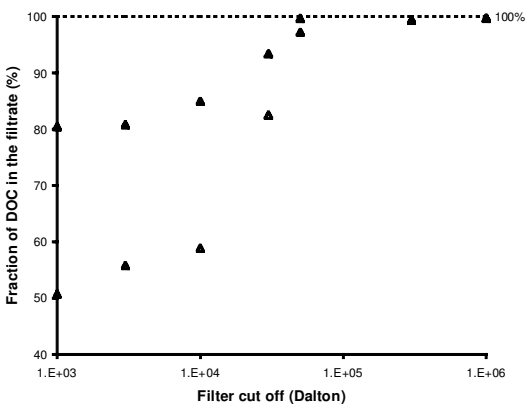

Figure 2. Evolution of the dissolved organic carbon (DOC) size distribution as a function of time for sample 516 (L/S = 80). Open and solid triangles show the DOC size-distribution after 74 days and 1 y reaction times, respectively.

Filter after 74 and 350 days reaction times, respectively (Figure 2).

Si and Al. The evolution of Si and Al concentrations with time was different for sample 447 when compared to the other three samples (Table 5). For sample 447, the initial increase of [Si] was followed by a decrease in the slope of the concentration curve for both L/S ratios. However, the slope was still positive after 1 y and no steady-state concentration was reached. For this sample, [Al] decreased after the initial increase to reach the same final [Al] for the two L/S ratios (6 mg/L). For the other three samples (490, 494 and 516), the evolution of Si and Al concentrations showed the same trend for both L/S ratios, the positive slope of the concentration curve decreasing with increasing time. Typical values were ~150–300 and 50–200 mg/L for Si and Al, respectively (Table 5). In addition, it is notable that there was a decrease of [Si] at the end of the experiment for sample 490 (L/S = 20) (Table 5).

The Al and Si concentrations in solution were not correlated with the presence of organic material as shown on Figure 3. In this figure, one may note that for sample 516 (L/S = 80, 350 days) Al and Si concentrations were constant whatever the filter cut off was. On the contrary, DOC concentration decreased with this parameter to indicate that Al and Si are present as aqueous species, rather than sorbed on organic colloids.

Na, K, Ca, Mg and Fe concentrations. After the initial fast decrease, [Na] and [K] were constant (~1400 and 5000 mg/L, respectively) throughout the experiment for the two L/S ratios (Table 5). In all experiments, the Ca, Mg and Fe concentrations were below the detection limit.

Evolution of pH. Contrasting pH evolutions as a function of time were observed for the different samples (Table 5). In samples 490, 494 and 516, the pH was constant throughout the experiment for both L/S ratios, whereas in sample 447, the pH decreased to 12.2 (L/S = 20) and to 12.9 (L/S = 80) at the end of the experiment (350 days).

Solids

SEM. The SEM analysis of sample 447 showed a strong dissolution of quartz in this initially quartz-rich sample. In all samples a small number of very fine blocky crystals can be found. These appear to be randomly distributed and to have a mixed Ca, Mg hydroxide composition. In most samples, limited precipitation of fibrous to honeycomb-textured CaAlSi-hydroxide phases (CASH) was also observed. Finally, rare occurrences of newly formed portlandite and brucite also appeared in most samples. Apart from the limited presence of these newly-formed phases, no significant textural modification was observed in the reacted clay samples.

X-ray diffraction. The XRD patterns obtained from reaction products are very similar to those of the initial raw materials, and in most cases no significant dissolution or neoformation was detected. Kaolinite and chlorite, whose proportions increase with depth in the sequence, showed no tendency to react during the experiments, whereas quartz disappeared in sample 447 for both L/S ratios. No significant modification of the clay mineralogy could be detected for samples 447 and 516 (Figure 4). On the contrary, a significant neoformation was observed for sample 494 (L/S = 20), the new phase being characterized by a rational series of basal reflections (d_{001} = 11.45 Å) which may be observed for the 74 and 350 days, reaction times experiments (L/S = 80, Figure 5). The saturation of this sample with different cations, its solvation with EG or its complete dehydration under secondary vacuum (10^{-5} Torr) did not alter its XRD pattern (Figure 6). Even though it was

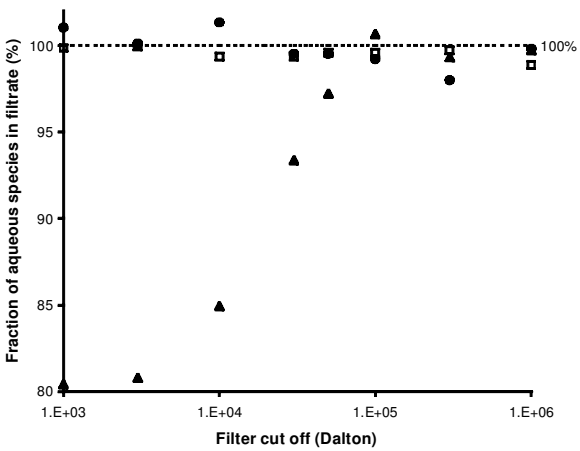

Figure 3. Distribution of aqueous species as a function of time for sample 516 after 1 y reaction time (L/S = 80). Si, Al and DOC are shown as open squares, solid circles, and solid triangles, respectively.

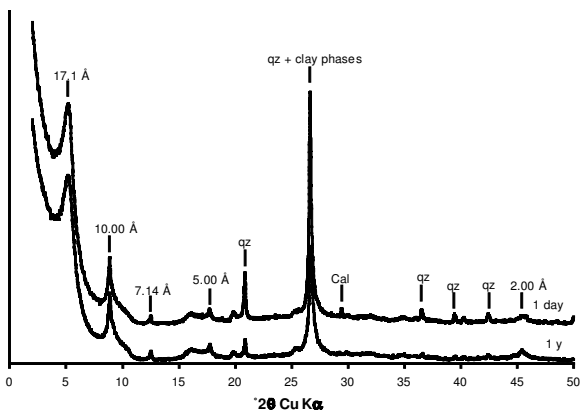

Figure 4. XRD patterns of sample 447 as a function of reaction time (L/S = 80 – Sr-saturation and EG solvation). The positions of the diffraction maxima are indexed. Quartz (qz) and calcite (Cal) impurities are labeled.

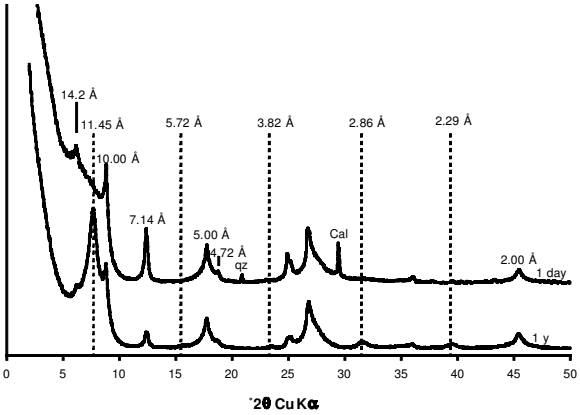

Figure 5. XRD patterns of sample 494 as a function of reaction time (L/S = 80 – Sr-saturation and ethylene glycol solvation). The positions of the diffraction maxima are indexed. Quartz (qz) and calcite (Cal) impurities are labeled. The rational series of reflections associated with the newly-formed tobermorite-like phase are shown as dashed lines.

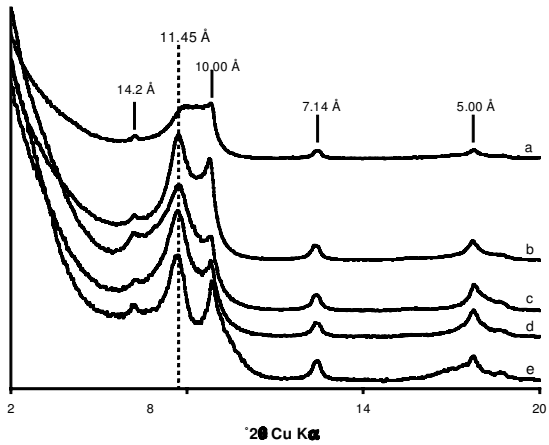

Figure 6. XRD patterns of sample 494 as a function of sample preparation (L/S = 80 – 1 y). The positions of the diffraction maxima are indexed, and the reflections attributed to the tobermorite-like phase are shown as dashed lines. (a) Na saturation and deep vacuum conditions (10^{-5} torr) during data collection, to ensure complete dehydration of expandable interlayers. (b) Na saturation and air-dried (AD) state. (c) Mg saturation and AD state. (d) Sr saturation and AD state. (e) Sr saturation and ethylene glycol solvation.

possible to reproduce the set of peak positions using a 2:1 layer with d_{001} = 11.45 Å, it was impossible to obtain a correct distribution of intensities between these reflections whatever the occupancy of the interlayer space. These reflections are more likely related to a newly-formed tobermorite-like phase (11 Å variety) which is reminiscent of the CASH phases observed using SEM.

A detailed study of XRD patterns recorded for sample 490 showed a continuous decrease of the smectite contribution at 17.3 Å with increasing reaction time, and the presence of a new peak at ~12.0 Å in the EG pattern (Figure 7). These modifications were more obvious for L/S = 80. In this case, the diffraction maximum at 12.0 Å is probably related to a phase different from that described for sample 494, because the series of reflections was not rational and because the contribution of this phase to the diffracted intensity varied as a function of sample state (cation saturation, EG solvation).

Application of the multi-specimen method indicates that after 1 y the reacted material is composed of five different phases. In addition to illite, chlorite and kaolinite which were initially present, two randomly interstratified MLM phases are also present. The first one with a 70% illite content and R = 0 ordering (random interstratification), is similar to the MLM phase present in the starting material (Claret, 2001). Fitting both AD and EG Sr-saturated patterns it was possible to estimate a 50% illite content for the other randomly interstratified MLM phase (Figure 8). In addition, the multi-specimen method confirmed the assumed disappearance of the initial smectite phase with reaction time.

Spectromicroscopic results. Spectroscopic investigation of untreated clay suspensions systematically showed the coexistence of K and C in the same area (Figure 9). To investigate these ubiquitous associations between K in clay minerals and C from organic matter, a detailed STXM study was carried out on sample 447 because the experimental alteration of this sample led to high DOC concentration in solution (Table 5). The absorption of the unaltered sample 447 was measured at the K L_3 edge (297.3 eV), above the C edge (Figure 10a). Dark gray values (regions 1–3) indicate a high combined absorption of K and C, showing large aggregates of clay-sized particles (~1 μm). The comparison of the ratio images of K (Figure 10b) and C (Figure 10c) distributions provided qualitative information on the relative contents of K and C, light gray values indicating high K or C content. The presence of high K concentrations over the

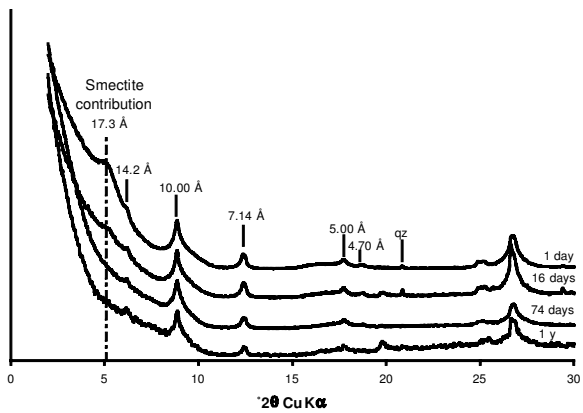

Figure 7. XRD patterns of sample 490 as a function of reaction time (L/S =80 – Sr saturation and EG solvation). The positions of the diffraction maxima are indexed, and quartz (qz) impurities are labeled. The position of the smectite contribution is shown as an irregular dashed line.

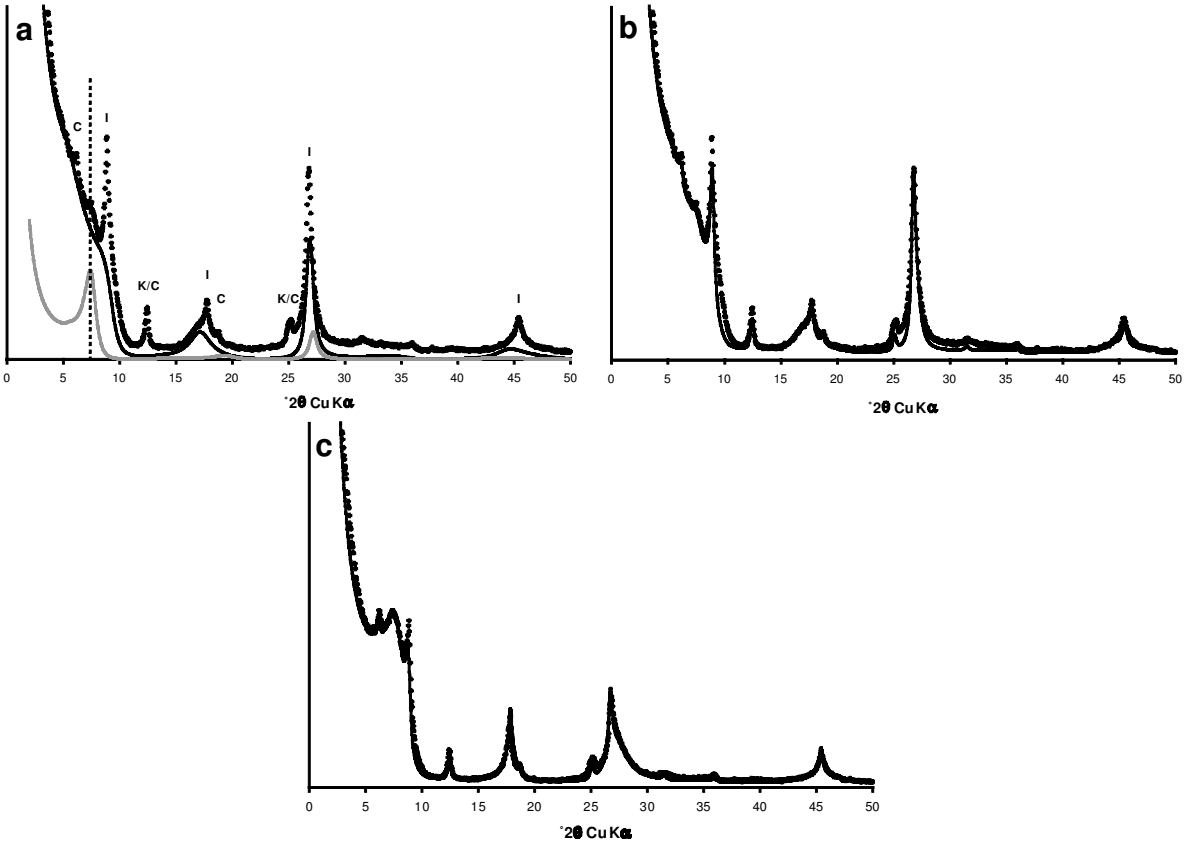

Figure 8. Mineralogical characterization of sample 490 (L/S = 80 – 1 y) using the multi-specimen method described by Sakharov *et al*. (1999). Experimental XRD patterns are shown as crosses, whereas calculated patterns are shown as solid lines. (a) Sr saturation and EG solvation. Contributions of the initial MLM phase with ~70% of illite layers and of the newly-formed MLM phase with ~50% illite layers are shown as solid and thin gray lines, respectively. The position of the latter contribution is shown as a dashed line. I, K and C labels indicate the positions of diffraction lines for illite, kaolinite, and chlorite respectively. (b) Sr saturation and EG solvation. Optimum fit to the experimental data is shown as a solid line. In addition to the two contributions from the MLM phases shown in part a, this calculated pattern includes that of discrete illite, kaolinite and chlorite. (c) Sr saturation and AD state. Optimum fit to the experimental data is shown as a solid line. The contributions to the diffracted intensity are similar to that in part b.

absorbing domains (regions 1–3) allowed their identification as K-rich phyllosilicates, such as the MLM, containing ~65% of non-expandable layers which makes up most of the clay-size fraction in all samples. Furthermore, these ratio images confirmed the association of organic material with these clays deduced from the XANES spectra (Figure 9). As shown by the similar distributions of K (Figure 10b) and C (Figure 10c), organic material covered clay plate surfaces and clay particle edges as well as inter-particle contacts for this unreacted sample. After reaction of sample 447 (350 days, L/S = 20), the contrast of the K ratio image (Figure 10e) is not as good as for the unreacted sample (Figure 10b). The concentration of this sample is very high and does not always allow a clear identification of the K contribution to the high global absorption (regions 4, 7). However, such an identification is possible in the low-absorption zones (regions 6, 8) of the reacted sample image. Furthermore, the unreacted sample was put in suspension in deionized water and, as a consequence, contained K only in the solid fraction. By contrast, both liquid and solid components of the reacted sample suspension in reacted SYF contain K, thus lowering the contrast (region 5). However, the identification of the large absorbing domains as K-rich phyllosilicates is beyond doubt.

In turn, the C ratio image of this reacted sample 447 (Figure 10f) showed a global depletion in the C content, and more especially a reduced amount of C on basal surfaces of clay particles whereas high C contents were still observed on particle edges and at inter-particle contacts (lighter gray values outlining regions 4 and 7). In particular, one may note that in the lower left corner of the reacted sample image (region 8) the K distribution is homogeneous (Figure 10e) whereas additional details (particle edges?) are visible on the C ratio image (Figure 10f).

Further investigation of the C (1s) absorption edge for untreated sample 447 showed characteristic features of aromatic carbon at 285 eV and 289 eV, carboxylic

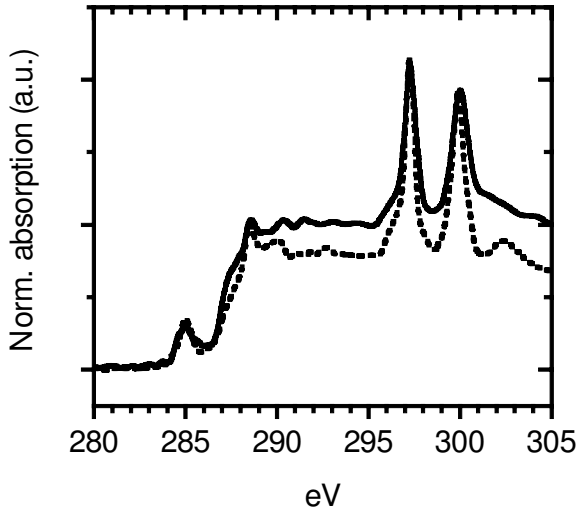

Figure 9. XANES spectra recorded at the carbon K-edge on unreacted sample 447 (solid line), and on sample 447 after 1 y reaction time (dashed line). The intensity is normalized to the L_3 absorption band of K at 297.3 eV. An additional peak at 300 eV corresponds to the L_2 absorption band of K (Henke *et al*., 1993).

groups at 289 eV and a broad shoulder at 287–288 eV (Table 6, Figure 9), which may be attributed either to a resonance of aromatic carbon bond to oxygen or to methyl and methylene groups of aliphatic carbon (Cody *et al*., 1995). The XANES spectrum (Figure 9) of reacted sample 447 (350 days in SYF; L/S 20) showed equivalent features with comparable intensities of absorption bands at 285 eV (aromatic carbon bonded to either proton or carbon) and at 289 eV (aromatic and/or aliphatic carboxylic acids).

Table 6. Assignment of energy bands to block building groups of organic matter.

Energy (eV)	Transition (s)	Functional group
285	1s-π*	$C_{arom.}$-C, $C_{arom.}$-H[a]
287	1s-π*	$C_{arom.}$-OH[a,b]
288	1s-3p/$\sigma_{C\text{-}H^*}$	CH_2, CH_3[c]
289	1s-π*	C=O, COOH, COOR[c,d,e]
	1s-2π*	$C_{arom.}$-H, $C_{arom.}$-C[b]
290	1s-4p	CH_2, CH_3[c]
291	1s-2π*	$C_{arom.}$-OH[e]
297	L_{III}	Potassium[f]
300	L_{II}	Potassium[f]

Note: [a](Hitchcock *et al*., 1992); [b](Francis and Hitchcock, 1992) [c](Hitchcock *et al*., 1986); [d](Ishii and Hitchcock, 1987); [e](Robin *et al*., 1988); [f](Henke *et al*., 1993)

After normalization to the K L_3-edge intensity, the continuum step of C absorption (*i.e.* the plateau after the absorption edge) decreased after 1 y reaction time to indicate that a smaller amount of organic material is associated with clay particles. However, this apparent decrease may be overestimated because of the different K concentrations in initial and reacted samples.

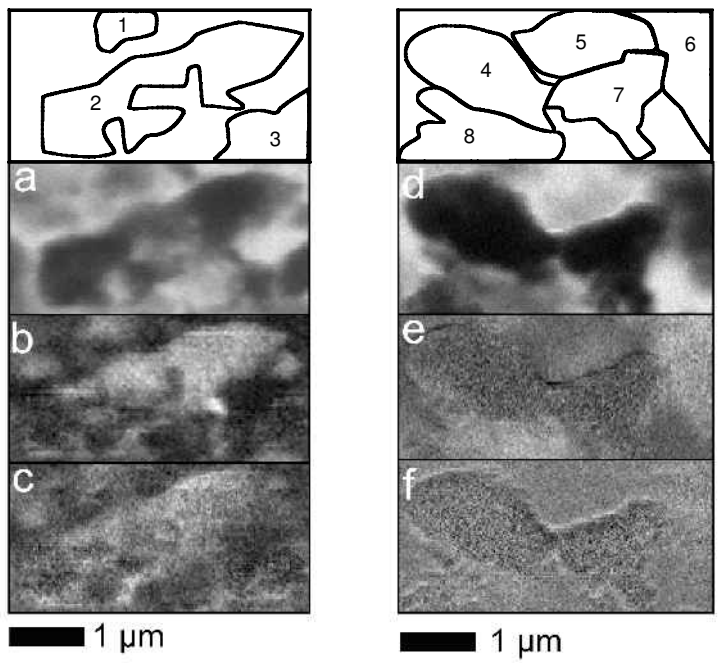

Figure 10. STXM images of unreacted sample 447 (a,b,c) and of sample 447 after 1 y reaction time with the Simple Young Fluid (L/S = 80 (d,e,f). The two sets of images are topped by a labeled sketch of the images for descriptive purposes (see text). Images 10a and 10d were taken at 297.3 eV. The dark gray values indicate a combined absorption by C and K. Images 10b and 10e are ratio images to visualize the distribution of K (E_{below} = Σ(280–290 eV), E_{above} = 297.3 eV). Images 10c and 10f are ratio images to visualize the distribution of C (E_{below} = 280 eV, E_{above} = Σ(285–290 eV)). The light gray values in ratio images indicate high K (b,e) or C (c,f) contents (see text).

DISCUSSION

Mineralogical evolution

The main goal of this experimental investigation was to determine the possible effects of basic solutions which might result from the initial alteration of concrete on the crystal chemistry of typical clays from the geological environment of the future French Meuse-Haute Marne underground laboratory. Such alteration of clays under low-to-moderate temperature and high-pH conditions was described previously by Eberl *et al*. (1993), Bauer and Berger (1998) and Bauer and Velde (1999). During their smectite alteration experiments, Bauer and Velde (1999) observed an initial decrease in the smectite CSDS followed by a decrease of the clay expandability via illite-smectite (I-S) MLM phases, *i.e.* illitization, in agreement with Eberl *et al*. (1993).

In our experiments, XRD pattern modeling indicates that a limited proportion of smectite transforms into a randomly interstratified MLM containing ~50% of illite layers after 1 y (L/S = 80). Indeed, XRD shows that in reacted sample 490, the amount of smectite, which was initially ~10% (Claret, 2001), decreases with reaction time simultaneously with the neoformation of this MLM phase (Figures 7, 8). On the other hand, no precipitation of this MLM phase or dissolution of smectite is observed in reacted samples 447 and 494 even though they initially contain discrete smectite. The contrasting scattering powers of the various phases present in the clay fraction may account for this apparent inconsistency as the presence of phases with high scattering powers in these samples could conceal the presence of a MLM phase similar to that identified in sample 490. For example, the presence of a newly-formed 11.45 Å tobermorite-like phase in sample 494 or the overwhelming intensity of smectite in sample 447 can impede the characterization of such a MLM phase. The very high scattering amplitude of the smectite phase may also conceal the possibility that it decreases with increasing reaction time if the initial discrete smectite is not strongly depleted as in sample 490.

The very high pH conditions of the experiments were found to be compatible with the neoformation of tobermorite-like phases in sample 494 (L/S = 80–74 days to 1 y terms) as these phases are usually formed under similar conditions during the binding process of Portland cements (Taylor, 1992). The SEM data indicate that this phase is present as traces in all altered samples although XRD detected its presence only in sample 494. At present there is no consistent explanation for the higher proportion of this tobermorite-like phase in altered sample 494.

In conclusion, except for the unusual precipitation of this tobermorite-like phase, the observed mineralogical evolution of clay minerals, and especially that of the discrete smectite phase, is compatible with earlier experiments (Eberl *et al*., 1993; Bauer and Velde, 1999) and leads to the formation of randomly interstratified MLM phases. However, one may note that the observed evolution is very limited and affects only the discrete smectite phase, leaving all other clay phases unaltered. In particular, the randomly interstratified MLM containing ~65% of illite layers which make up most of the clay-size fraction (Claret, 2001) and the discrete illite phase seem unaltered in all experiments. In addition, the discrete smectite phase is only partly affected, as its decreasing proportion could be observed only for sample 490 which initially contained ~10% of this phase (Table 2). This decrease was undetectable for sample 447 which initially contained ~20% of discrete smectite, probably because of the high scattering amplitude of this phase. On the contrary, the evolutions described in the literature affect all of the smectite phase (Eberl *et al*., 1993; Bauer and Velde, 1999). The origin of such a limited reactivity of clay phases when in contact with alkaline solutions will be discussed below.

Evolution of solution chemistry

Except for sample 447 for which the observed pH drop was induced by the dissolution of micro-crystalline quartz, the solution pH did not change significantly throughout the experiments. Consistent with the limited mineralogical evolution of clays, this steady pH indicates that there is no significant fluid-clay reaction as a pH drop is expected as a result of clay-fluid interaction because of the speciation of Al^{3+} and Si^{4+}. Chermak (1992) measured such a drop, from 12.91 down to 6.68, of the quenched pH in his batch experiments with fine-grained Opalinus Shale (35 days, 200°C). Decarreau (1999) also observed such a pH drop in the experiments conducted with samples from the Callovo-Oxfordian formation in alkaline solution. After one week, depending on starting solution, the pH decreased from 12.6 to 7.0 or from 13.5 to 10 as a result of the OH^- consumption. One may note that in these experiments the limited liquid:solid ratio (3:1) enhanced this pH drop. Bauer and Berger (1998) observed the same evolution of solution pH in the batch experiments at 35 and 80°C for kaolinite and smectite, respectively, for initial KOH concentrations below 0.1 M.

The limited reactivity of clays is confirmed by the rather low Si and Al concentrations measured in solution. The only high [Si] value (4134 mg/L), which was measured for sample 447, results from the dissolution of micro-crystalline quartz. All other measured values are similar, or lower, to that measured by Bauer and Berger (1998) in KOH 0.1 M solution (initial *in situ* pH 11.47 at 80°C).

The initial interlayer cation (Ca^{2+}) is likely to have been exchanged rapidly for K^+ at the beginning of the reaction as shown by the initial reduction of [K^+] in solution. Liberated Ca, as well as that introduced in the initial SYF solution, are not retrieved in solution, and probably precipitated as CASH or tobermorite-like

phases, which were observed by SEM. This hypothesis is supported by the systematic dissolution of calcite traces in reacted sample 494 in which the tobermorite-like phase was observed (not shown).

Influence of organic matter

The measured increase of DOC concentration with reaction time indicates that the organic material is much more affected than clays by alkaline solutions. This was expected as treatment with basic NaOCl solutions, for example, is recommended to remove organic material from clay samples (Moore and Reynolds, 1989). With increasing reaction time, organic matter in solution is gradually decomposed as shown by the evolution of the DOC size-distribution (Figure 2).

The STXM investigations indicate that the organic material is preferentially released from the basal surfaces of clay particles whereas the edges of these particles are still covered after one year. As will be discussed below, it is likely that this specific reactivity of the organic clay coverage is responsible for the observed limited alteration of clay minerals in the present high-pH experiments. This hypothesis is supported by the strong dissolution features observed by SEM on mineral species, *e.g.* quartz, which were not initially covered by organic material.

Because of the preferential desorption of the organic material from their basal surfaces, an important proportion of clay particle surface area is accessible to alkaline solution after several months of reaction. However, in spite of this increased direct contact surface between the clay minerals and the solution, the evolution of these minerals remains very limited. Bauer and Berger (1998) explained contrasting reactivity observed between kaolinite and smectite in high molar KOH solutions at 35 and 80°C by structural considerations and emphasized the main role of crystal edges. The essential role played by crystal edges in the alteration process of clay minerals may also account for the low alteration rate observed in our experiments, as access to these edges is blocked by organic material throughout the experiments as shown by STXM investigations.

The dominant influence of edge surface sites on the dissolution rate has also been demonstrated for biotite based on macroscopic experiments conducted at low pH (Turpault and Trotignon, 1994). Consistently, Bosbach *et al.* (2000) observed that the proton-promoted dissolution of hectorite particles takes place exclusively at the crystal edges, the basal surfaces being completely unreactive on the experiment time scale. Furthermore, crystal edges are readily blocked by the presence of organic material as demonstrated by Chin and Mills (1991). The latter authors showed clearly that the presence in solution of humic acids from soils (50 mg L^{-1}) inhibit kaolinite dissolution, and hypothesized that large humic acid molecules bind to multiple surface Al sites preventing the adsorption of both H^+ and small organic ligands. Such a passivation of the reactive clay edges by organic material coverage was demonstrated by Taubald *et al.* (2000) who showed that chlorite which is unstable under oxidizing conditions showed no tendency to react during their experiment.

CONCLUSIONS

The effect of alkaline solutions on clay mineralogy was investigated experimentally at 60°C as a function of time to mimic the effect of a pH plume resulting from the alteration of cements on the clay formation hosting the future French underground laboratory. From the three clay phases initially present, *i.e.* discrete smectite, discrete illite, and a randomly-interstratified MLM phase containing ~65% of illite layers, only the smectite was shown to transform. The evolution of discrete smectite to a randomly interstratified MLM phase containing ~50% of illite layers is consistent with earlier similar experiments (Eberl *et al.*, 1993; Bauer and Velde, 1999). The neoformation of a tobermorite-like phase was the only additional significant mineralogical evolution.

Coverage of clay mineral outer surfaces, and more especially of the crystal edges, may be responsible for the very limited character of the observed mineralogical transformation by blocking the access of the alkaline solution to these most reactive sites. After 1 y of reaction time, the bonding of organic ligands to crystal edges is still effective whereas basal surfaces appear to be free of the initial organic coverage. As a result, aqueous concentration of DOC is high but does not promote clay mineral dissolution by complexing Al or Si. The average size of this colloidal organic material tends to decrease with increasing reaction progress.

At lower pH values than those used in this study (*e.g.* 7–8) such humic material may influence the sorption of metal ions, and more especially that of actinides. Their complexation both in solution and on solid surfaces will be an essential parameter for their fate.

ACKNOWLEDGMENTS

The results presented in the present article were collected during a PhD thesis granted by Andra (French National Agency for Nuclear Waste Disposal). Andra is thanked for permission to publish this manuscript. BL and FC acknowledge financial support from Andra. Spectromicroscopic data were collected using the X-1A STXM developed by the group of Janos Kirz and Chris Jacobsen at SUNY Stony Brook, with support from the Office of Biological and Environmental Research, U.S. DoE under contract DE-FG02-89ER60858, and from the NSF under grant DBI-9605045. The zone plates were developed by Steve Spector and Chris Jacobsen of Stony Brook and Don Tennant of Lucent Technologies Bell Labs with support from the NSF, under grant ECS-9510499.

REFERENCES

Anderson, K., Allard, B., Bengtsson, M. and Magnusson, B. (1989) Chemical composition of cement pore waters. *Cement and Concrete Research*, **19**, 327–332.

Bauer, A. and Berger, G. (1998) Kaolinite and smectite dissolution rate in high molar KOH solutions at 35°C and 80°C. *Applied Geochemistry*, **13**, 905–916.

Bauer, A. and Velde, B. (1999) Smectite transformation in high molar KOH solutions. *Clay Minerals*, **34**, 259–273.

Bauer, A., Velde, B. and Berger, G. (1998) Kaolinite transformation in high molar KOH solutions. *Applied Geochemistry* , **13**, 619–629.

Berner, U. (1990) *A Thermodynamic Description of the Evolution of Porewater Chemistry and Uranium Speciation during the Degradation of Cement*. Nagra NTB, Report 90-12, Baden, Switzerland.

Bosbach, D., Charlet, L., Bickmore, B. and Hochella, M.F. (2000) The dissolution of hectorite: In-situ, real-time observations using atomic force microscopy. *American Mineralogist* , **85**, 1209–1216.

Bouchet, A. and Rassineux, F. (1997) *Echantillons d'Argiles du Forage EST 104: Etude minéralogique Approfondie*. Andra, Report DR-P-0ERM-98-007A, Chatenay-Malabry, France, 107 pp.

Cama, J., Ganor, J., Ayora, C. and Lasaga, A.C. (2000) Smectite dissolution kinetics at 80 degrees C and pH 8.8. *Geochimica et Cosmochimica Acta*, **64**, 2701–2717.

Carroll, S.A. and Walther, J.V. (1990) Kaolinite dissolution at 25°, 60° and 80°C. *American Journal of Science*, **290**, 797–810.

Carroll-Webb, S.A. and Walther, J.V. (1988) A surface complex reaction model for the pH-dependence of corundum and kaolinite dissolution. *Geochimica et Cosmochimica Acta*, **52**, 2609–2623.

Cassagnabere, A., Parneix, J.C., Sammartino, S., Griffault, L., Maeder, U. and Milodowski, T. (2001) Mineralogical evolution of bitumimous marl adjacent to an alkaline water conducting feature at the Maqarin analogue site. Pp. 367–370 in: *Water-Rock Interaction* (R. Cidu, editor). Balkema, Liss, Tokyo.

Chermak, J.A. (1992) Low temperature experimental investigation of the effect of high pH NaOH solutions on the Opalinus shale, Switzerland. *Clays and Clay Minerals*, **40**, 650–658.

Chermak, J.A. (1993) Low temperature experimental investigation of the effect of high pH KOH solutions on the Opalinus shale, Switzerland. *Clays and Clay Minerals*, **41**, 365–372.

Chin, P.F. and Mills, G.L. (1991) Kinetics and mechanisms of kaolinite dissolution: effect of organic ligands. *Chemical Geology*, **90**, 307–317.

Claret, F. (2001) Caractérisation structurale des transitions minéralogiques dans les formations argileuses: Contrôles et implications géochimiques des processus d'illitisation. Cas particulier d'une perturbation alcaline dans le Callovo-Oxfordien Laboratoire souterrain Meuse-Haute-Marne. PhD thesis, Université Joseph Fourier, Grenoble, France, 174 pp.

Cody, G.D., Botto, R.E., Ade, H., Behal, S., Disko, M. and Wirick, S. (1995) Inner-shell spectroscopy and imaging of a subbituminous coal: In-situ analysis of organic and inorganic microstructure using C(1s)-, Ca(2p)-, and Cl(2s)-NEXAFS. *Energy and Fuels*, **9**, 525–533.

Decarreau, A. (1999) *Etude Expérimentale des Réactions entre Argiles de sites de Stockage Français et Eaux Cimentaires*. Andra, Report D-RP-1UPT-99-001, Chatenay-Malabry, France, 38 pp.

Drits, V.A. and Sakharov, B.A. (1976) *X-ray Structure Analysis of Mixed-layer Minerals*. Doklady Akademii Nauk, SSSR, Moscow, 256 pp.

Drits, V.A., Środoń, J. and Eberl, D.D. (1997) XRD measurement of mean crystallite thickness of illite and illite/smectite: Reappraisal of the Kübler index and the Scherrer equation. *Clays and Clays Minerals*, **45**, 461–475.

Eberl, D.D., Velde, B. and McCormick, T. (1993) Synthesis of illite-smectite from smectite at Earth surface temperatures and high pH. *Clay Minerals*, **28**, 49–60.

Faure, P., Landais, P. and Griffault, L. (1999) Behavior of organic matter from Callovian shales during low-temperature air oxidation. *Fuel*, **78**, 1515–1525.

Francis, J.T. and Hitchcock, A.P. (1992) Inner-shell spectroscopy of p-benzoquinone, hydroquinone, and phenol: Distiguishing quinoid and benzenoid structures. *Journal of Physical Chemistry*, **96**, 6598–6610

Haworth, A., Sharland, S.M. and Tweed, C.J. (1989) Modeling of the degradation of cement in a nuclear waste repository. *Material Research Society Symposium Proceedings*, **127**, 447–454.

Henke, B.L., Gullikson, E.M. and Davis, J.C. (1993) X-ray interactions: Photoabsorption, scattering, transmission, and reflection at E=50–30000 eV, Z=1–92. *Atomic Data and Nuclear Data Tables*, **54**, 181–342.

Hitchcock, A.P. and Mancini, D.C. (1994) Bibliography and database of inner-shell excitation spectra of gas phase atoms and molecules. *Journal of Electron Spectroscopy and Related Phenomena*, **67**, 1–132.

Hitchcock, A.P., Newbury, D.C., Ishii, I., Stöhr, J., Horsley, J.A., Redwing, R.D., Johnson, A.L. and Sette, F. (1986) Carbon K-shell excitation of gaseous and condensed cyclic hydrocarbons: C_3H_6, C_4H_8, C_5H_8, C_5H_{10}, C_6H_{10}, C_6H_{12}, and C_8H_8. *Journal of Chemical Physics*, **85**, 4849–4862.

Hitchcock, A.P., Urquart, S.G. and Rightor, E.G. (1992) Inner shell spectroscopy of benzaldehyde, terephthalaldehyde, ethyl benzoate, terephthaloyl chloride, and phosgene: Models for core excitation of poly (ethylene terephathalate). *Journal of Physical Chemistry*, **96**, 8736–8750.

Huang, W.L. (1993) The formation of illitic clays from kaolinite in KOH solution from 225°C to 350°C. *Clays and Clay Minerals*, **41**, 645–654.

Huertas, F.J., Caballero, E., de Cisneros, C.J., Huertas, F. and Linares, J. (2001) Kinetics of montmorillonite dissolution in granitic solutions. *Applied Geochemistry*, **16**, 397–407.

Inoue, A., Bouchet, A., Velde, B. and Meunier, A. (1989) Convenient technique for estimating smectite layer percentage in randomly interstratified illite/smectite minerals. *Clays and Clay Minerals*, **37**, 227–234.

Ishii, I. and Hitchcock, A.P. (1987) A quantitative experimental study of the core excited electronic states of foramide, formic acid, and formyl fluoride. *Journal of Chemical Physics*, **87**, 830–839.

Jacobsen, C., Williams, S., Anderson, E., Browne, M.T., Buckley, C.J., Kern, D., Kirz, J., Rivers, M. and Zhang, X. (1991) Diffraction-limited imaging in a scanning transmission x-ray microscope. *Optics Communications*, **86**, 351–364.

Jacobsen, C., Wirick, S., Flynn, G. and Zimba, C. (2000) Soft X-ray spectroscopy with sub-100 nm spatial resolution. *Journal of Microscopy*, **197**, 173–184.

Jeffries, N.L., Tweed, C.J. and Wisbey, S.J. (1988) The effects of changes in pH in a clay surrounding a cementitious repository. *Material Research Society Symposium Proceedings* , **112**, 43–52.

Lunden, I. and Andersson, K. (1989) Modelling the mixing of cement pore water and groundwater using the PHREEQC code. *Material Research Society Symposium Proceedings*, **127**, 949–956.

Ma, Y., Chen, C.T., Meigs, G., Randall, K. and Sette, F. (1991) High-resolution K-shell photoabsorption measurements of simple molecules. *Physical Review A*, **44**, 1848–1858.

Mohnot, S.M., Bae, J.H. and Foley, W.L. (1987) A study of alkali/mineral reactions. *SPE Reservoir Engineering*, 653–663.

Moore, D.M. and Reynolds, R.C., Jr. (1989) *X-ray Diffraction*

and the Identification and Analysis of Clay Minerals. Oxford University Press, Oxford and New York, 322 pp.

Nagra (1995) *Column Experiments: Results of Experiments and Modelling*. Nagra NTB, Report 95–70, Baden, Switzerland.

Neuhäusler, U., Abend, S., Jacobsen, C. and Lagaly, G. (1999) Soft X-ray spectromicroscopy on solid-stabilized emulsions. *Colloid Polymer Science*, **277**, 719–726.

Rassineux, F., Griffault, L., Meunier, A., Berger, G., Petit, S., Viellard, P., Zellagui, R. and Munoz, M. (2001) Expandability-layer stacking relationship during experimental alteration of a Wyoming bentonite in pH 13.5 solutions at 35 and 60°C. *Clay Minerals*, **36**,197–210.

Reardon, E.J. (1990) An ion interaction model for the determination of chemical equilibrium in cement/water systems. *Cement and Concrete Research*, **20**, 175–192.

Robin, M.B., Ishii, I., McLaren, R. and Hitchcock, A.P. (1988) Fluorination effects on the inner shell spectra of unsaturated molecules. *Journal of Electron Spectroscopy and Related Phenomena*, **47**, 53–92.

Sakharov, B.A., Lindgreen, H., Salyn, A. and Drits, V.A. (1999) Determination of illite-smectite structures using multispecimen X-ray diffraction profile fitting. *Clays and Clays Minerals*, **47**, 555–566.

Spector, S., Jacobsen, C. and Tennant, D. (1997) Process optimization for production of sub-20 nm soft X-ray zone plates. *Journal of Vacuum Science and Technology B*, **15**, 2872–2876.

Taubald, H., Bauer, A., Schafer, T., Geckeis, H., Satir, M. and Kim, J.I. (2000) Experimental investigation of the effect of high-pH solutions on the Opalinus Shale and the Hammerschmiede Smectite. *Clay Minerals*, **35**, 515–524.

Taylor, H.F.W. (1992) Tobermorite, jennite, and cement gel. *Zeitschrift für Kristallographie*, **202**, 41–50.

Turpault, M.P. and Trotignon, L. (1994) The dissolution of biotite single crystals in dilute HNO_3 at 24°C: Evidence of an anisotropic corrosion process of micas in acidic solutions. *Geochimica et Cosmochimica Acta*, **58**, 2761–2775.

Velde, B., Suzuki, T. and Nicot, E. (1986) Pressure-temperature-composition of illite/smectite mixed-layer minerals: Niger delta mudstones and other examples. *Clays and Clay Minerals*, **34**, 435–441.

Viellard, P. and Rassineux, F. (1992) Thermodynamic and geochemical modelling of the alteration of two cement matrices. *Applied Geochemistry*, **1**, 125–136.

Winn, B., Ade, H., Buckley, C., Howells, M., Hulbert, S., Jacobsen, C., Kirz, J., McNulty, I., Miao, J., Oversluizen, T., Pogorelsky, I. and Wirick, S. (1996) X1A: second generation undulator beamlines serving soft x-ray spectromicroscopy experiments at the NSLS. *Reviews of Scientific Instruments* , **67**, 1–4.

Wolery, T.J. (1983) *EQ3NR a computer program for geochemical aqueous speciation-solubility calculations: User's guide and documentation*. Lawrence Livermore National Laboratory UCRL-53414, Livermore, CA, USA, 202 pp.

Zhang, X., Ade, H., Jacobsen, C., Kirz, J., Lindaas, S., Williams, S. and Wirick, S. (1994) Micro-XANES: chemical contrast in the scanning transmission x-ray microscope. *Nuclear Instruments and Methods in Physics Research A*, **347**, 431–435.

(*Received 6 December 2001; revised 29 March 2002; Ms. 612; A.E. David A. Laird*)